DOI: 10.1002/ejic.200600821

Efficient DNA Cleavage Induced by Copper(II) Complexes of Hydrolysis Derivatives of 2,4,6-Tri(2-pyridyl)-1,3,5-triazine in the Presence of Reducing Agents

Joaquín Borrás,*[a] Gloria Alzuet,[a] Marta González-Alvarez,[a] Jose L. García-Giménez,[a] Benigno Macías,[b] and Malva Liu-González[c]

Keywords: Copper triazine complexes / Oxidative DNA damage / ROS scavengers / Oxidation

The reaction of 2,4,6-tri(pyridyl)-1,3,5-triazine (ptz) and copper(II) salts in dmf/water (1:1) results in the hydrolysis of ptz and formation of the anions bis(2-pyridylcarbonyl)amide (ptO_2^-) and bis(2-pyridylamine)amide (ptN_2^-), which are found in the complexes $[Cu(ptN_2)(OAc)]\cdot 3H_2O$ (**1**), $[Cu(ptO_2)(OAc)(H_2O)]\cdot H_2O$ (**2**), $[Cu(ptN_2)(for)]\cdot 3H_2O$ (**3**) (for = formate), $[Cu(ptO_2)(for)(H_2O)]$ (**4**), $[Cu(ptO_2)(benz)]\cdot H_2O$ (**5**) (benz = benzoate), and $[Cu(ptO_2)F(H_2O)]_2\cdot 3H_2O$ (**6**). This report includes the chemical and spectroscopic characterization of all these complexes along with the crystal structures of **4**–**6**. The coordination spheres of Cu^{II} in **4** and **5** are best described as distorted tetragonal square pyramidal for the former and distorted square planar for the latter. The crystal structure of **6** shows the presence of two discrete monomeric $[Cu(ptO_2)F(H_2O)]$ entities in the crystallographic asymmetric unit in which both copper(II) ions have a distorted square-pyramidal coordination geometry. The binding of the complexes to DNA has been investigated with the aid of viscosity and thermal denaturation studies, both of which indicate that the interaction is probably due to the outer-sphere mechanism. The ability of the compounds to cleave DNA has also been tested. Efficient oxidative cleavage was observed in the presence of a mild reducing agent (ascorbate) and dioxygen. Mechanistic studies with reactive oxygen species (ROS) scavengers confirm that hydrogen peroxide, the hydroxyl radical, singlet oxygen-like species, and the superoxide anion are necessary diffusible intermediates in the scission process. A mechanism involving either the Fenton or the Haber–Weiss reaction plus the formation of copper oxene species is proposed for the DNA cleavage mediated by these compounds.

Introduction

The interaction of reactive oxygen species (ROS) with DNA is of considerable interest because of the potential pathobiological significance of ROS-induced DNA damage. Such damage may be promutagenic and has been linked to the pathogenesis of human diseases such as cancer and aging.[1,2]

The transition metal ion catalyzed reduction of hydrogen peroxide has served as a useful model reaction for generating ROS. Reduction of H_2O_2 by copper ion produces highly reactive DNA-damaging species.[3] Copper ion induces significantly more DNA base damage in the presence of H_2O_2 than does ferrous ion, the other biologically relevant transition metal ion.[4,5] Moreover, copper is an important structural metal ion in chromatin,[6–8] which contains about one copper ion per kilobase.[6] For these reasons, there is an increased interest in the ability of copper ion to participate in DNA-damaging reactions in vivo.[8,9]

Kinetic,[9–11] inhibitor,[4,5,9] and sequence-context[12–15] studies have all suggested that DNA damage induced by copper ion in the presence of H_2O_2 occurs site-specifically at the sites of DNA-associated copper. However, the nature of the last DNA-oxidizing species produced by the interaction of the DNA-Cu^I complex with H_2O_2 remains uncertain. Some investigators have suggested that the hydroxyl radical is the principal reactive intermediate,[9,16] while others have proposed less reactive intermediates such as an oxidocopper complex[11,14,15] or cupryl ion.[10] Regardless of the true nature of the reaction mechanism, exposure of DNA to copper has been reported to result in single- and double-strand breaks, modified bases, abasic sites, and DNA-protein crosslinks.[17,18]

2,4,6-Tri(2-pyridyl)-1,3,5-triazine (ptz; Scheme 1) is of current interest due to its utility as a spacer for designing multinuclear metal complexes. Compounds of this family of 2,4,6-triaryltriazines are usually stable against hydrolysis;

[a] Departament de Química Inorgànica, Facultat de Farmàcia, Universitat de València,
Vicent Andrés Estellés s/n, 46100 Burjassot, Spain
Fax: +34-963-544-960
E-mail: Joaquin.Borras@uv.es
[b] Departamento de Química Inorgánica, Facultad de Farmacia, Universidad de Salamanca
Campus Unamuno, 37007 Salamanca, Spain
[c] SCSIE, RX. Universitat de València,
50 Dr. Moliner, 46100 Burjassot, Spain

Supporting information for this article is available on the WWW under http://www.eurjic.org or from the author.

indeed, their hydrolysis requires the presence of a concentrated mineral acid and temperatures above 150 °C.[19] Lerner and Lippard[20,21] have found that ptz undergoes hydrolysis in the presence of Cu^{II} in aqueous media. They have also reported the crystal structure of a copper(II) complex with a hydrolysis product of ptz. On the basis of the Cu–N bond lengths and angles of the carbonyl carbon atoms within the chelate ring, they suggested that the coordination of ptz induces an angular strain which allows a nucleophilic attack at the carbon atoms of the triazine ring by the solvent, which, in turn, results in the hydrolysis of ptz.[20,22] Kinetic and thermodynamic data have revealed that such a reaction probably occurs by nucleophilic attack at the triazine ring by OH^- or H_2O.[23] However, a comparison of the structural and NMR spectroscopic data of rhodium and ruthenium complexes with ptz and a ptz derivative have led to the conclusion that a decrease in electron density at the carbon atoms of the triazine ring due to the electron-withdrawing effect (L→M) of the metal ion is a more predominant factor than angular strain in the metal-assisted hydrolysis of ptz.[24,25] Very recently, Li et al. have confirmed by a theoretical study that the hydrolysis of ptz is affected by the electron-withdrawing effect of the metal ions.[26]

The hydrolysis of ptz (Scheme 1) involves the formation of several intermediates containing either two imino nitrogens (ptN_2^-), one imino and one carbonyl ($ptNO^-$), and finally two carbonyl groups (ptO_2^-). The literature contains reports of metal complexes of the ptO_2^- ligand, usually described as $bpca^-$, which is formed upon deprotonation of bis(2-pyridylcarbonyl)amine (Hbpca; Scheme 1). Mono-, di- (homo- and heteronuclear), and trinuclear complexes have been reported for various divalent and trivalent metal ions (M^{II} = Cu^{II}, Fe^{II}, Mn^{II}, Co^{II}, Ni^{II}, and Zn^{II}; M^{III} = Fe^{III}, Rh^{III}).[27–33] Among these, a ternary complex of copper(II) with one $bpca^-$ and another derivative formed during the hydrolysis process, namely 2-picolinamide, has been described.[28] The ptO_2^- anion is obtained by means of a Cannizzaro-type reaction of pyridine-2-carboxaldehyde and NaNCO in the presence of copper metal ion.[34] Kawijara et al. have described the ptN_2^- ligand,[35] which forms when ptz is mixed with copper(II) acetate at reflux in dry MeOH in the presence of $NaClO_4$. This ligand links the copper(II) ions to form a polymer chain.

In this paper we describe the crystal structures of copper(II) complexes with ptO_2^- and other new copper complexes with ptN_2^-. The ptz and the ptz-derived ligands present a planar structure and can interact with the bases of DNA through stacking, which is one of the well-known conditions for interaction with DNA in order to give rise to ROS that then cleave the DNA. In this vein, Thorp et al.[36] have reported the DNA-cleavage activity of Ru^{II}-ptz complexes based on the formation of oxidoruthenium(IV). Our group has also published numerous papers about the nuclease activity of copper(II) complexes in the presence of reducing agents.[37–42] In this paper we assay the nuclease activity of the synthesized copper(II) complexes in the presence of reducing agents such as mercaptopropionic acid, ascorbic acid, and glutathione.

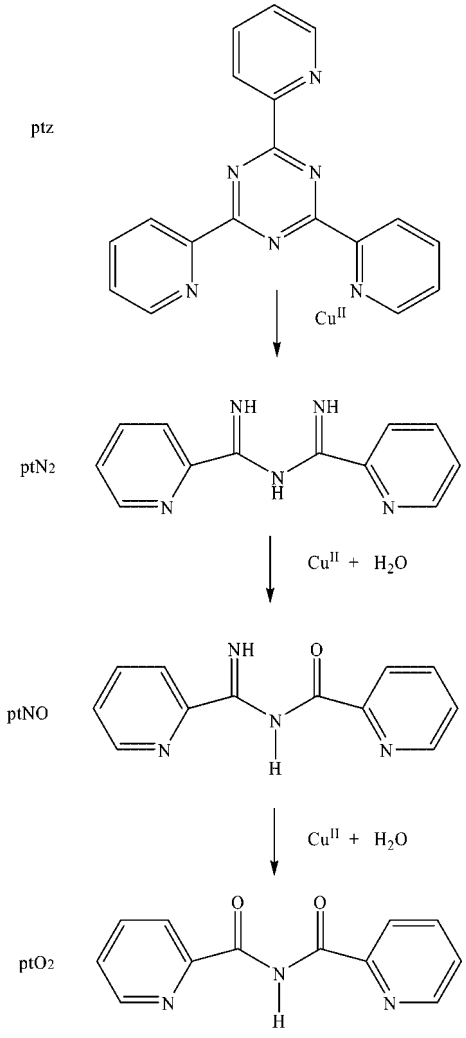

Scheme 1. Hydrolysis of 2,4,6-tri(2-pyridyl)-1,3,5-triazine.

Results and Discussion

Synthesis

The reaction of copper salts and ptz in dmf/H_2O (4:1) resulted in the hydrolysis of ptz to ptO_2^- or ptN_2^- anions and afforded complexes of composition $[Cu(ptO_2)(X)(H_2O)]$, $[Cu(ptN_2)(X)]\cdot 3H_2O$ (X = acetate or formate), $[Cu(ptO_2)(benz)]\cdot H_2O$, and $[Cu(ptO_2)(F)(H_2O)]_2\cdot 3H_2O$.

Crystal Structures

[Cu(ptO$_2$)(for)(H$_2$O)] (4)

Figure 1 shows an ORTEP view of the molecule with the atomic numbering scheme. Selected bond lengths and angles are listed in Table 1. The coordination sphere of copper(II) is best described as a distorted tetragonal square pyramid, as can be deduced from the τ value of 0.24.[43] The basal positions are occupied by the three nitrogen atoms of the ptO_2^- ligand and one oxygen atom of the monodentate formate (for) anion. The apical site is occupied by the oxygen atom from the coordinated water molecule. The Cu–N

bond lengths, which range from 1.942(3) to 2.022(2) Å, are very similar to those found in other previously reported copper(II) complexes with ptO_2^-.[27] The Cu–O_{for} and the Cu–O_{water} bond lengths are 1.933(2) and 2.329(4) Å, respectively. The four basal atoms are quasi coplanar, and the copper ion is displaced 0.106 Å below the plane. The second oxygen of the formate group is located a long distance away from copper(II) [2.882(4) Å].

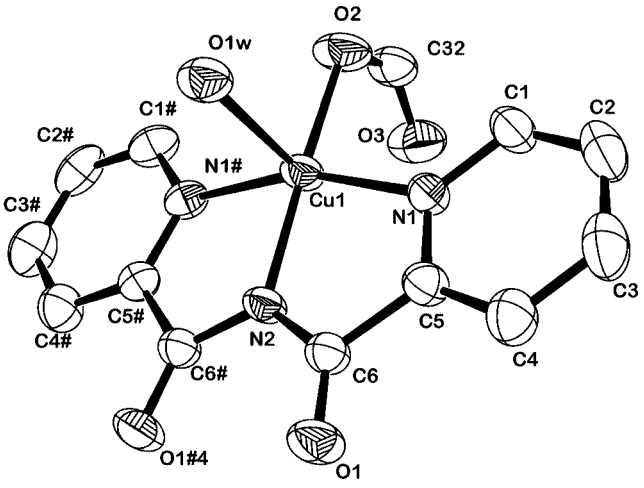

Figure 1. ORTEP drawing of [Cu(ptO_2)(for)(H_2O)] (**4**).

The crystal packing is stabilized by intermolecular hydrogen bonds. A moderate hydrogen bond is formed between O1W and O3 of the formate anion [O1W···O3 2.792(5) Å, O1W–H1A–O3 174.92(4.60)°]. In addition, O1W forms a moderately strong hydrogen bond with the carbonyl O1 [O1W···O1 2.944(3) Å, O1W–H1B–O1 137.56(6)°].[44]

[Cu(ptO_2)(benz)]·H_2O (5)

An ORTEP view of the complex with the atom numbering scheme is shown in Figure 2. Selected bond lengths and angles are listed in Table 1. The geometry of the copper(II) ion can be described as distorted square planar. The coordination polyhedron is formed by a ptO_2^-, which functions as a tridentate ligand through the nitrogen atoms, and one carboxylate O atom from the benzoate (benz) ligand. The three Cu–N bond lengths, which are within the range 1.9268(13)–2.0007(16) Å, are similar to those of the complex described above and to those found for other copper(II) ptO_2 complexes.[27] The distortion of the square-planar geometry can be determined by the dihedral angle between the CuN_2 and CuNO planes. When the dihedral angle is 0° the geometry is planar while when the angle is 90° the stereochemistry is tetrahedral. In this complex, the dihedral angle value of 3.48(6)° indicates a very slightly distorted square planar configuration. A distorted square pyramid could be considered due to fact that the Cu–O4

Table 1. Selected bond lengths [Å] and angles [°] for [Cu(ptO_2)(for)(H_2O)] (**4**), [Cu(ptO_2)(benz)]·H_2O (**5**), and [Cu(ptO_2)F(H_2O)]$_2$·3H_2O (**6**).[a]

[Cu(ptO_2)(for)(H_2O)] (**4**)		[Cu(ptO_2)(benz)]·H_2O (**5**)		[Cu(ptO_2)F(H_2O)]$_2$·3H_2O (**6**)	
Cu(1)–O(2)	1.933(2)	Cu(1)–O(3)	1.9268(13)	Cu(1)–N(2A)	1.87(2)
Cu(1)–N(2)	1.942(3)	Cu(1)–N(2)	1.9279(14)	Cu(1)–F(1)	1.933(12)
Cu(1)–N(1)	2.022(2)	Cu(1)–N(1)	1.9927(15)	Cu(1)–N(3A)	1.95(3)
Cu(1)–N(1)#1	2.022(2)	Cu(1)–N(3)	2.0007(16)	Cu(1)–N(1A)	2.02(2)
Cu(1)–O(1W)#2	2.329(4)	Cu(1)–O(4)	2.690(2)	Cu(1)–O(1)	2.290(10)
				Cu(2)–F(2)	1.902(11)
				Cu(2)–N(2B)	1.94(2)
				Cu(2)–N(3B)	1.98(2)
				Cu(2)–N(1B)	2.03(2)
				Cu(2)–O(2)	2.283(11)
O(2)–Cu(1)–N(2)	176.2(3)	O(3)–Cu(1)–N(2)	178.09(6)	N(2A)–Cu(1)–F(1)	173.1(6)
O(2)–Cu(1)–N(1)	98.28(6)	O(3)–Cu(1)–N(1)	99.37(7)	N(2A)–Cu(1)–N(3A)	80.0(13)
N(2)–Cu(1)–N(1)	81.46(6)	N(2)–Cu(1)–N(1)	82.13(7)	F(1)–Cu(1)–N(3A)	98.3(10)
O(2)–Cu(1)–N(1)#1	98.28(6)	O(3)–Cu(1)–N(3)	96.25(6)	N(2A)–Cu(1)–N(1A)	82.7(16)
N(2)–Cu(1)–N(1)#1	81.46(6)	N(2)–Cu(1)–N(3)	82.19(6)	F(1)–Cu(1)–N(1A)	97.8(11)
N(1)–Cu(1)–N(1)#1	161.35(12)	N(1)–Cu(1)–N(3)	164.01(6)	N(3A)–Cu(1)–N(1A)	160.6(13)
O(2)–Cu(1)–O(1W)#2	91.25(19)			N(2A)–Cu(1)–O(1)	91.2(6)
N(2)–Cu(1)–O(1W)#2	92.51(17)			F(1)–Cu(1)–O(1)	95.5(4)
N(1)–Cu(1)–O(1W)#2	94.08(9)			N(3A)–Cu(1)–O(1)	94.5(7)
N(1)#1–Cu(1)–O(1W)#2	94.08(9)			N(1A)–Cu(1)–O(1)	94.7(5)
				F(2)–Cu(2)–N(2B)	170.2(6)
				F(2)–Cu(2)–N(3B)	102.6(10)
				N(2B)–Cu(2)–N(3B)	77.5(14)
				F(2)–Cu(2)–N(1B)	94.1(12)
				N(2B)–Cu(2)–N(1B)	84.3(13)
				N(3B)–Cu(2)–N(1B)	160.5(14)
				F(2)–Cu(2)–O(2)	95.5(4)
				N(2B)–Cu(2)–O(2)	94.2(6)
				N(3B)–Cu(2)–O(2)	94.3(7)
				N(1B)–Cu(2)–O(2)	94.0(6)

[a] Symmetry transformations used to generate equivalent atoms: #1 x, y, $-z + 2$; #2 $x + 1$, y, z.

distance is 2.690(2) Å. In this case, the carboxylate acts as a bidentate ligand, in contrast to that observed for $[Cu(ptO_2)(for)(H_2O)]$ (**4**) and for the previously reported complex $[Cu(ptO_2)(OAc)(H_2O)]\cdot H_2O$.[27] The four basal atoms deviate slightly from planarity, and the copper ion is displaced 0.037 Å below the plane.

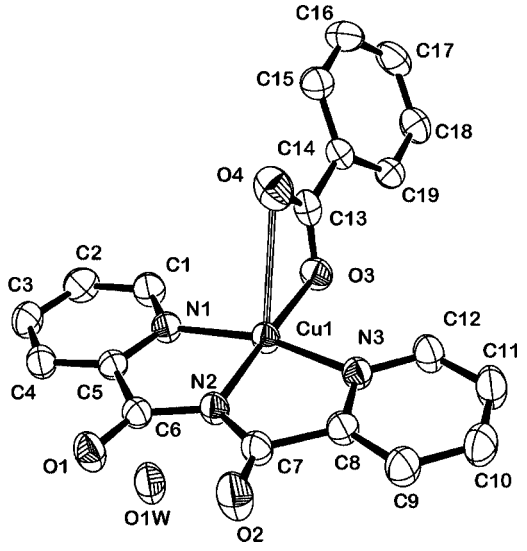

Figure 2. ORTEP drawing of $[Cu(ptO_2)(benz)]\cdot H_2O$ (**5**).

The molecule is stabilized by moderate and weak hydrogen bonds formed by O1W and two O carbonyl groups [O1W···O1 3.112(3) Å, O1W–H1A–O1 129.67(2.35)°; O1W···O2 2.858(2) Å, O1W–H1A–O2 150.18(2.45)°; O1W···O1 3.112(3) Å, O1W–H1B–O1 101.46(2.35)°].[44]

$[Cu(ptO_2)F(H_2O)]_2\cdot 3H_2O$ (6)

Figure 3 displays the structure of complex $[Cu(ptO_2)F(H_2O)]_2\cdot 3H_2O$ with the labeling scheme. Selected interatomic distances and angles are listed in Table 1. The crystal structure shows the presence of two discrete monomeric $[Cu(ptO_2)F(H_2O)]$ entities and three lattice water molecules in the crystallographic asymmetric unit. Both copper(II) ions have a distorted square-pyramidal coordination geometry. The equatorial planes are defined by three nitrogen atoms of the ptO_2^- ligand [Cu–N in the range 1.87(2)–2.02(2) Å for Cu(1) and 1.94(2)–2.03(3) Å for Cu(2)] and one fluoride anion [Cu(1)–F(1) 1.933(12), Cu(2)–F(2) 1.902(11) Å]. The apical position is occupied by the O atom of a water molecule [Cu(1)–O1 2.290(10), Cu(2)–O2 2.283(11) Å]. The equatorial plane displays a slight tetrahedral distortion as Cu(1) is displaced 0.1407 Å below the plane while Cu(2) lies 0.1559 Å above the plane. These two monomeric $[Cu(ptO_2)F(H_2O)]$ entities show different trigonality parameters (τ). These different τ values − 0.24 for Cu(1) and 0.16 for Cu(2) − are due to crystal packing effects.

The CuN_3F plane in each entity is coplanar to the ptO_2^- ligand [angle between planes of 179.74° in Cu(1) and 178.63° in Cu(2)]. Moreover, both $[Cu(ptO_2)F(H_2O)]$ entities are also coplanar (the angle between the $Cu1N_3F$ and $Cu2N_3F$ planes is 178.70°).

The crystal structure is stabilized by many hydrogen-bonding interactions involving the fluoride anions (F1, F2), the oxygen atoms of the ptO_2^- ligand (O2, O3), and the oxygen atoms of the water molecules (O1W, O2W, and O3W), some of which are of moderate strength.[44]

Spectroscopic Properties

The IR spectra of $[Cu(ptN_2)(for)]\cdot 3H_2O$ (**3**; violet) and $[Cu(ptO_2)(for)(H_2O)]$ (**4**; blue) are significantly different (see Figure S1 in the Supporting Information). Thus, while the presence of a strong band at 1712 cm^{-1}, attributable to the ν(C=O) vibrations characteristic of the ptO_2^- ligand,[27] is a significant feature in the IR spectrum of **4**, the IR spectrum of **3** does not show this band but rather shows a band

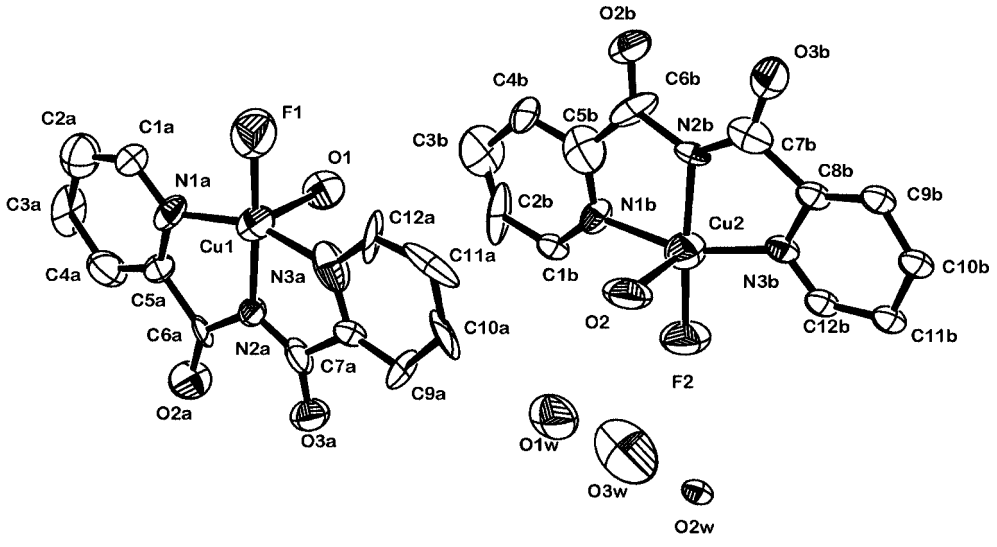

Figure 3. ORTEP drawing of $[Cu(ptO_2)F(H_2O)]_2\cdot 3H_2O$ (**6**).

at 1666 cm^{-1} due to the δ(N–H) vibrations. Another domain in which noteworthy differences exist between the IR spectra of both complexes is that between 3500 and 3000 cm^{-1}. For example, in the spectrum of **4**, a strong band with two peaks is observed at 3500 and 3440 cm^{-1}, attributable to ν(O–H) vibrations of the water molecules, while in the IR spectrum of **3** two bands appear at 3300 and 3100 cm^{-1}. These can most likely be assigned to ν(N–H) and ν(O–H) vibrations of the lattice water molecules, respectively. Both spectra exhibit bands at 1600 and 1350 cm^{-1} that correspond to the $\nu_{as}(COO^-)$ and $\nu_s(COO^-)$ vibrations of the formate group.

The interpretation of the IR spectrum of **4** is corroborated by the corresponding IR spectra of $[Cu(ptO_2)(benz)]\cdot H_2O$ (**5**) and $[Cu(ptO_2)F(H_2O)]_2\cdot 3H_2O$ (**6**), which both show the strong band at 1712 cm^{-1} and the two peaks at 3500 and 3440 cm^{-1}. In contrast, the IR spectrum of $[Cu(ptN_2)(OAc)]\cdot 3H_2O$ (**1**) shows no bands at 3500, 3440, or 1712 cm^{-1}, but rather at 3300, 3100, and 1660 cm^{-1}, similar to those of $[Cu(ptN_2)(for)]\cdot 3H_2O$ (**3**). In the IR spectrum of **5**, the bands attributable to the $\nu_{as}(COO^-)$ and $\nu_s(COO^-)$ vibrations of the benzoate group appear at 1600 and 1350 cm^{-1}, respectively.

Differences between complexes **3** and **4** are also found in their reflectance spectra. Thus, while the spectrum of **4** shows an unresolved broad d–d band at about 637 nm, that of **3** presents the d–d transition at about 565 nm. The same pattern is observed for the d–d bands of **2** (620 nm) and **1** (565 nm). Complexes **5** and **6** show the d–d band at 582 and 627 nm, respectively. The position of the d–d maximum thus follows the order **5** < **2** < **6** < **4**. The order of the d–d maximum position for the three latter complexes is in good agreement with the extent of geometrical distortion defined by the τ parameter: 0.16 (**2**), 0.16 and 0.24 (**6**), and 0.24 (**4**). In addition to the d–d band, a shoulder appears at about 420 nm in complexes **2**, **4**, and **5**; this can be assigned to an LMCT band. While the spectrum for the complex **1** does not exhibit this band, that of **6** shows a very strong band at 400 nm that can be attributed to an F–Cu LMCT band.

As the complexes are soluble in H_2O, we also recorded their UV/Vis spectra in aqueous solution. The spectra of aqueous solutions of complexes **5**, **2**, and **4** show the same maxima at 646 nm (ε = 45, 91, and 90 $M^{-1}cm^{-1}$, respectively), thus suggesting that all three compounds contain the same chromophore in solution. The shift of the d–d band position with respect to that in the diffuse reflectance spectra is probably a consequence of the coordination of water molecules and the dissociation of the carboxylate anions. Moreover, a weak LMCT band at about 400 nm, similar to that observed in the solid-state spectra, is present, which indicates the interaction between the metal ion and the ptO_2^- anion. Finally, the UV/Vis spectrum of an aqueous solution of complex **1**, while showing a band at 590 nm (ε = 49 $M^{-1}cm^{-1}$), shows none around 400 nm (see Figure S2 in the Supporting Information), thus confirming the results in the solid state.

EPR Spectroscopy

The X- and Q-band spectra of polycrystalline samples of the complexes were recorded at room temperature. Powder samples of **2**, **4**, **5**, and **6** were prepared from the single crystals. The EPR parameters obtained by simulation with WINSimphonia[45] are given in Table 2. The Q-band EPR spectrum of **5** is the axial-only spectrum, with $g_\parallel > g_\perp$. This indicates a mainly copper(II) $d_{x^2-y^2}$ orbital ground state. The other Q-band EPR spectra are rhombic, with $g_x < g_y < g_z$ and R values ranging from 0.07 to 0.38, which suggests that the unpaired electron is in the $d_{x^2-y^2}$ orbital. The pattern of the EPR spectra is in good agreement with the square-planar geometry of **5** and the square-pyramidal geometry of **4** and **6**. Interestingly, the better resolution of the Q-band spectra allowed us to deduce the rhombic nature of the EPR spectrum of **2**, which had been hypothesized to be axial in a previous paper.[27]

It is also interesting to note that the EPR spectra of the complexes with the ptO_2^- ligands (**2** and **4**) are different from those of the complexes with the ptN_2^- ligand (**1** and **3**; see Figure S3 in the Supporting Information).

Mass Spectral Analysis

The FAB spectra of complexes **2**, **4**, **5**, and **6** show a major peak at *m*/*z* 289 that corresponds to the $[Cu(ptO_2)]^+$ fragment due to the dissociation of the carboxylate or F^- anions. There are, however, other significant peaks in the spectra. The FAB spectrum of **2**, for example, shows peaks at *m*/*z* 349 and 307 attributable to the $[Cu(ptO_2)(OAc) + H]^+$ and $[Cu(ptO_2) + H_2O]^+$ fragments. The FAB mass spectrum of **6**, which is similar to that of **2**, shows a peak at *m*/*z* 309 that can be attributed to the $[Cu(ptO_2)F + H]^+$ fragment. The FAB spectrum of complex **4** displays a peak at *m*/*z* 335 that corresponds to the $[Cu(ptO_2)(for)H]^+$ entity. The FAB spectrum of **5** shows a peak at *m*/*z* 411 that is

Table 2. X- and Q-band EPR data for the complexes.

Compound	Q-band				X-band			
	g_x	g_y	g_z	R	$g_\parallel$	$g_\perp$	$g_\parallel$	$g_\perp$
$[Cu(ptN_2)(OAc)]\cdot 3H_2O$ (**1**)	2.045	2.062	2.217	0.11			2.060	2.208
$[Cu(ptO_2)(OAc)(H_2O)]\cdot H_2O$ (**2**)	2.046	2.049	2.230	0.07			2.211	2.060
$[Cu(ptN_2)(for)]\cdot 3H_2O$ (**3**)	2.043	2.064	2.216	0.14			–	–
$[Cu(ptO_2)(for)(H_2O)]$ (**4**)	2.044	2.064	2.238	0.17			2.063	2.19
$[Cu(ptO_2)(benz)]\cdot H_2O$ (**5**)	–	–	–	–	2.207	2.046	2.191	2.056
$[Cu(ptO_2)F(H_2O)]\cdot H_2O$ (**6**)	2.047	2.094	2.218	0.38			–	–

assigned to the $[Cu(ptO_2)(benz) + H]^+$ fragment. Interestingly, the mass spectrum of **1** presents a peak at *m*/*z* 305, which corresponds to the $[Cu(ptN_2) + H_2O]^+$ fragment. The presence of this peak agrees with the difference in mass between ptO_2^- (226.06) and ptN_2^- (224.09).

Electrochemical Behavior

In the electroactivity domain of acetonitrile/Bu_4NClO_4, the cyclic voltammograms of complexes **2** and **5** have the same shape. A reduction peak is observed around –0.90 mV (vs. SCE) towards cathodic potentials; this can be attributed to the reduction of Cu^{II} to Cu^{I}. The same E_{cat} value for both complexes indicates that **2** and **5** give identical species in acetonitrile solution, probably the $[Cu(ptO_2)]^+$ entity, thus confirming the UV/Vis and FAB data. On the reverse scan, an anodic peak was found at about –0.2 mV. The voltammogram is clearly irreversible, probably because the Cu^{I} species formed upon reduction of Cu^{II} is unstable. The reduction peak at –0.90 mV relative to SCE corresponds to –0.68 mV relative to NHE. Such a value indicates a higher stabilization of the Cu^{II} species with respect to those of Cu^{I}.

Attempts to determine the electrochemical behavior of the complexes in cacodylate buffer, the medium used in the biological studies, were unsuccessful because a solid precipitated in the electrolytic cell.

DNA-Binding Interactions

The mode and propensity of binding of the complexes to calf-thymus DNA (CT-DNA) were studied with the aid of various techniques.

Viscosity Measurements

Viscosity measurements were carried out on CT-DNA by varying the concentration of the complexes. Hydrodynamic measurements that are sensitive to length changes are regarded as the least ambiguous and most critical tests of binding in solution. One classic intercalation model results in the lengthening of the DNA helix as the base-pairs are separated to accommodate the binding ligand, thus leading to the increase of DNA viscosity. In contrast, complexes that bind exclusively in DNA grooves by means of partial and/or nonclassical intercalation under the same conditions typically cause either a less pronounced change (positive or negative) of DNA solution viscosity or none at all.[46] The results obtained with our compounds reveal that the presence of complexes **3**, **5**, or **6** has no effect on the relative viscosity of CT-DNA. This indicates that the interaction of these complexes follows the general pattern of complexes that bind in DNA grooves by either a partial or nonclassical intercalation.

Thermal Denaturation

In order to obtain a better understanding of the interaction of the compounds, the binding of complexes **3**, **5**, and **6** to CT-DNA was studied by examining the thermal denaturation profile of DNA. The melting temperature (T_m) of CT-DNA upon addition of **3**, **5**, or **6** was found to be 75.7, 78.5, and 75.6 °C respectively. The complexes thus produce no increase in T_m upon addition to DNA (T_m = 76.6 °C in cacodylate buffer 0.1 M, NaCl 2 mM, pH 6.0). These results suggest that the complexes do not effect duplex stabilization through intercalation between the DNA base-pairs.

In summary, both viscosity and T_m measurements indicate that the complexes do not intercalate between the DNA base-pairs. Most probably, the interaction of the complexes is mainly electrostatic through the phosphate backbone of the DNA since the compounds are present in solution as the positive $[Cu(ptO_2)]^+$ or $[Cu(ptN_2)]^+$ species.

Nuclease Activity of Complexes and Mechanistic Investigations

Oxidative DNA Cleavage Mediated by the Compounds

The ability of complexes **1**–**6** to cleave DNA was investigated by means of gel electrophoresis with supercoiled pUC18 in 0.1 M cacodylate buffer (pH 6.0) and with ascorbate activation. Control experiments with $CuSO_4$ were also carried out under the same experimental conditions. The DNA cleavage activity of the complexes was assayed by the conversion of supercoiled DNA (SC, form I) to nicked circular (NC, form II) or linearized DNA (LC, form III). All the complexes were found to exhibit nuclease activity (Figure 4). At 6, 18, and 30 μM the compounds present the same cleavage pattern (lanes 2–4, parts a–f of Figure 4). The fact that the complexes exhibit similar nuclease activity is not surprising since they are dissociated in solution into $[Cu(ptO_2)]^+$ or $[Cu(ptN_2)]^+$. The $[Cu(ptO_2)]^+$ or $[Cu(ptN_2)]^+$ entities derived from the complexes must therefore be the active species that mediate DNA-strand scission since $CuSO_4$ at the highest concentration assayed is only able to produce a partial conversion of SC DNA into NC DNA (lane 6, Figure 4, g). Thus, the DNA cleavage activity of the compounds can be ascribed to the cooperative effect between Cu^{II} and the ptO_2^- or ptN_2^- ligands.

Because certain copper(II) complexes are able to bring about hydrolytic cleavage of DNA, the possibility of a hydrolytic mechanism for the DNA damage mediated by these compounds must be taken into account. In order to clarify this point, the nuclease activity of complexes **1**–**6** was assayed without ascorbate activation. No DNA cleavage was observed, which indicates that a hydrolytic mechanism is not involved (lane 1, parts a–f of Figure 4).

The nuclease efficiency of a large number of Cu^{II} complexes is known to depend on the reducing agent used for initiating the DNA cleavage. We thus tested the activity of **4** in the presence of various activators [ascorbate, hydrogen peroxide, 3-mercaptopropionic acid (MPA), and glutathione] at a 50-fold excess relative to the complex concentration. The results, shown in Figure 5 (A), indicate the following increasing order of efficiency: hydrogen peroxide < glutathione < MPA < ascorbate (cf. lanes 8, 10, 12, and 14 in Figure 5, A). By way of comparison, the same assays were

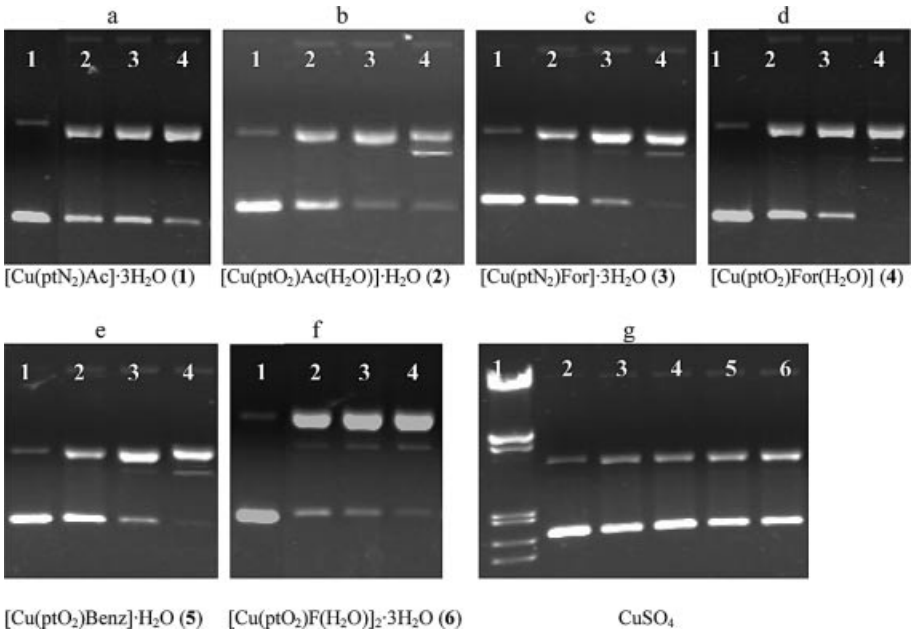

Figure 4. Agarose gel electrophoresis of pUC18 plasmid DNA treated with the complexes or $CuSO_4$ with [ascorbate]:[tested compound] = 100:1 or without ascorbate. Incubation time: 1 h (37 °C). (a) $[Cu(ptN_2)(OAc)]\cdot 3H_2O$ (**1**), (b) $[Cu(ptO_2)(OAc)(H_2O)]\cdot H_2O$ (**2**) (c) $[Cu(ptN_2)(for)]\cdot 3H_2O$ (**3**), (d) $[Cu(ptO_2)(for)(H_2O)]$ (**4**), (e) $[Cu(ptO_2)(benz)]\cdot H_2O$ (**5**), (f) $[Cu(ptO_2)F(H_2O)]_2\cdot 3H_2O$ (**6**), (g) $CuSO_4$; **a**–**f**: lane 1: 60 μM complex without ascorbate; lane 2: 6 μM complex with ascorbate 100×; lane 3: 18 μM complex with ascorbate 100×, 30 μM complex with ascorbate 100×; **g**: lane 1: λDNA/EcoRI + Hind III Marker; lane 2: supercoiled DNA; lane 3: supercoiled DNA with 3 mM ascorbate; lane 4: 6 μM $CuSO_4$ with ascorbate 100×; lane 5: 18 μM $CuSO_4$ with ascorbate 100×; lane 6: 30 μM $CuSO_4$ with ascorbate 100×.

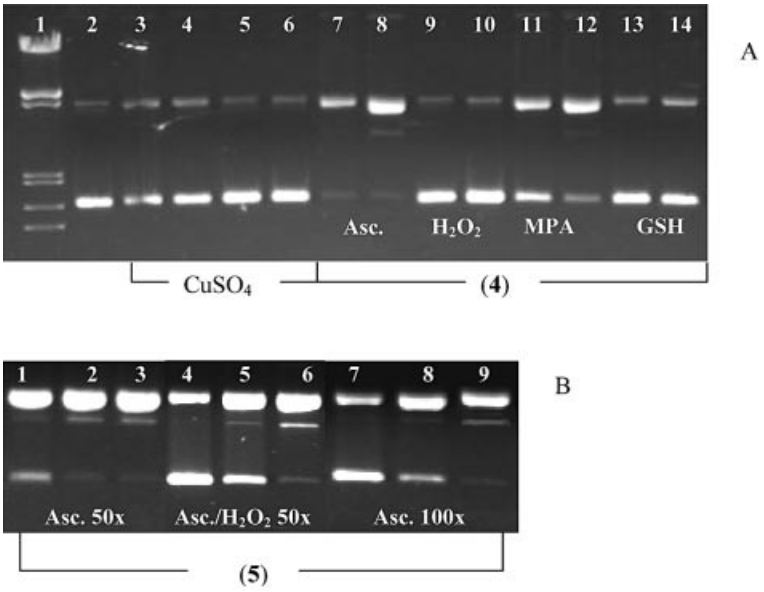

Figure 5. A) Agarose gel electrophoresis of pUC18 plasmid DNA treated with $[Cu(ptO_2)(for)(H_2O)]$ (**4**) in the presence of different reducing agents. Incubation time: 1 h (37 °C). Lane 1: λDNA/EcoRI + Hind III Marker; lane 2: supercoiled DNA; lane 3: $CuSO_4$ 30 μM + ascorbate 50×; lane 4: $CuSO_4$ 30 μM + H_2O_2 50×; lane 5: $CuSO_4$ 30 μM + MPA 50×; lane 6: $CuSO_4$ 30 μM + glutathione 50×; lane 7: **4** 18 μM + ascorbate 50×; lane 8: **4** 30 μM + ascorbate 50×; lane 9: **4** 18 μM + H_2O_2 50×; lane 10: **4** 30 μM + H_2O_2 50×; lane 11: **4** 18 μM + MPA 50×; lane 12: **4** 30 μM + MPA 50×; lane 13: **4** 18 μM + glutathione 50×; lane 14: **4** 30 μM + glutathione 50×. B) Agarose gel electrophoresis of pUC18 plasmid DNA treated with $[Cu(ptO_2)(benz)]\cdot H_2O$ (**5**) in the presence of ascorbate and ascorbate/H_2O_2. Incubation time: 1 h (37 °C). Lane 1: **5** 6 μM + ascorbate 50×; lane 2: **5** 18 μM + ascorbate 50×; lane 3: **5** 30 μM + ascorbate 50×; lane 4: **5** 6 μM + ascorbate/H_2O_2 50×; lane 5: **5** 18 μM + ascorbate/H_2O_2 50×; lane 6: **5** 30 μM + ascorbate/H_2O_2 50×; lane 7: **5** 6 μM + ascorbate 100×; lane 8: **5** 18 μM + ascorbate 100×; lane 9: **5** 30 μM + ascorbate 100×.

performed with $CuSO_4$. Lanes 3–6 (Figure 5, A) show that $CuSO_4$ at 30 μM is not an efficient chemical nuclease in the presence of these activating agents. Several authors have studied the influence of different reducing agents on the cleavage of DNA by copper(II) complexes.[47–50] Sigman et al.,[47] for example, examined the influence of the activating agent on the nuclease activity of a bis(*o*-phenanthroline)-copper(II) complex and deduced that ascorbic acid and 3-mercaptopropionic acid are the most efficient reducing agents. However, while these same authors found MPA to be superior to ascorbic acid because it produces less background cleavage, in our study ascorbic acid is clearly more efficient than MPA. Chiou et al.[48] have indicated that ascorbate is more effective in cleaving DNA than other reducing agents such as MPA and dithiothreitol even though the latter compounds possess higher reducing powers than ascorbate. The uniqueness of ascorbate as a reducer in the scission reaction may depend on its ability to generate hydrogen peroxide in the presence of oxygen and metal ions, whereas other reducing agents with a thiol group are known to produce superoxide, which rapidly undergoes dismutation in aqueous solution. Detmer et al.[49] have found that a combination of ascorbate and H_2O_2 is a more effective activating agent than ascorbate alone. In order to elucidate the influence of mixing ascorbate with H_2O_2, the cleavage process of **5** was studied with ascorbate/H_2O_2 (50×) or ascorbate (50× and 100×) as activators (Figure 5, B). No significant differences in DNA damage were found.

Mechanistic Studies

The mechanism of pUC18 DNA cleavage by the compounds was studied using inhibiting reagents. The results for complexes **3** and **5** are shown in Figure 6. The involvement of ROS was investigated with standard hydroxyl radical scavengers (DMSO, *tert*-butyl alcohol, potassium iodide, and urea), singlet oxygen scavengers (azide and DABCO), superoxide radical scavengers (Tiron), and catalase. The groove binding preferences were tested in the presence of the minor groove binder distamycin and the major groove binder methyl green. The reduction of Cu^{II} to Cu^{I} during the cleavage process was evaluated with neocuproine, a ligand that chelates strongly to copper(I).

A strong inhibition of DNA cleavage mediated by **5** is observed upon addition of DMSO, *tert*-butyl alcohol, potassium iodide, or urea, thereby indicating that hydroxyl radical is involved in the cleavage process (lanes 4–7, Figure 6, A). The addition of sodium azide or DABCO (lanes 8 and 9, Figure 6, A) also decreases the cleavage efficiency, which indicates that either $^1O_2$ or a singlet-oxygen-like entity is one of the active oxygen intermediates responsible for the cleavage. The inhibitory activity of sodium azide can be ascribed to the affinity of the azide anion for transition metals.[51] Adding Tiron to the reaction mixture decreases the DNA damage slightly, which suggests that the superoxide anion is involved in the DNA scission (lane 10, Figure 6, A). Catalase also inhibits the nucleolytic process, which confirms that hydrogen peroxide is also necessary in the DNA strand scission (lane 14, Figure 6, A).

Treatment of pUC18 DNA with distamycin prior to the addition of **5** has no effect on the cleavage reaction mediated by the compound (lane 11, Figure 6, A). In contrast, prior treatment with methyl green attenuates the DNA strand scission (lane 12, Figure 6, A). It can thus be inferred from these results that **5** prefers major groove binding. Finally, neocuproine does not inhibit the DNA damage (lane 13, Figure 6, A). This is probably due to the strong redox stability of the $[Cu(ptO_2)]^+$ species, as was deduced from the electrochemical studies.

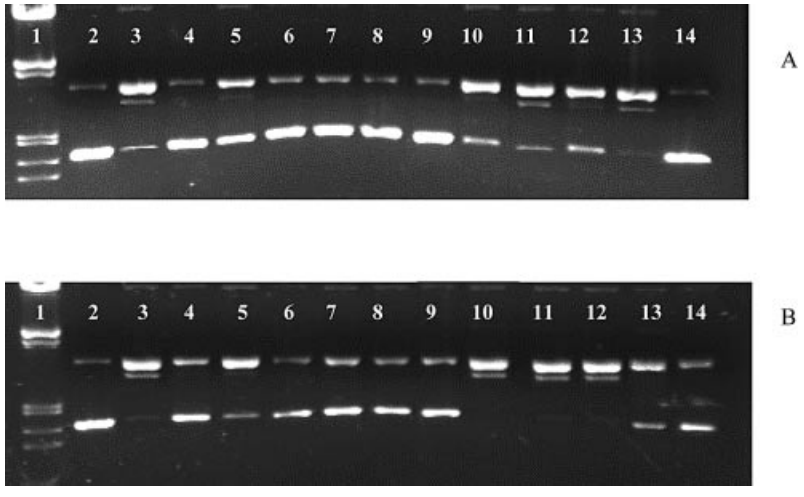

Figure 6. A) Agarose gel electrophoresis of pUC18 plasmid treated with 30 μM $[Cu(ptO_2)(benz)]\cdot H_2O$ (**5**) and 1.5 mM ascorbate/H_2O_2 in the presence of potential inhibitors. Incubation time: 1 h (37 °C). B) Agarose gel electrophoresis of pUC18 plasmid treated with 30 μM $[Cu(ptN_2)(for)]\cdot 3H_2O$ (**3**) and 1.5 mM ascorbate/H_2O_2 in the presence of potential inhibitors. Incubation time: 1 h (37 °C). Lane 1: λDNA/EcoRI + Hind III Marker; lane 2: supercoiled DNA; lane 3: complex without inhibitors; lane 4: complex + DMSO (1 M); lane 5: complex + *tert*-butyl alcohol (1 M); lane 6: complex + IK (0.4 M); lane 7: complex + urea (0.4 M); lane 8: complex + NaN_3(100 mM); lane 9: complex + DABCO (0.4 M); lane 10: complex + Tiron (10 mM); lane 11: complex + distamycin (8 μM); lane 12: complex + methyl green (2.5 μL of a 0.01 mg mL^{-1} solution); lane 13: complex + neocuproine (75 μM); lane 14: complex + catalase (6.5 units).

The results for complex **3** (Figure 6, B) indicate that, as was the case for **5**, hydroxyl radical, $^1O_2$, and hydrogen peroxide are the active species responsible for the DNA damage (lanes 4–7, 8, 9, and 14, Figure 6, B). However, the cleavage scission process mediated by this compound is somewhat different from that of **5**. First of all, the superoxide anion does not seem to be involved in the DNA scission (lane 10, Figure 6, B). Also, since neocuproine attenuates the DNA cleavage in this case (lane 13, Figure 6, B), it seems likely that the reduction of Cu^{II} to Cu^{I} takes place, probably due to a lower stability of $[Cu(ptN_2)]^+$ with respect to that of $[Cu(ptO_2)]^+$. Moreover, in contrast to **5**, complex **3** does not show major or minor groove binding preferences (lanes 11 and 12, Figure 6, B).

The involvement of hydroxyl radicals was subjected to further studies. The hydroxyl release by **5** was studied by using 2-deoxy-D-ribose as a radical trap.[52] 2-Deoxy-D-ribose provides a chemically equivalent model for the oxidative target in DNA strand scission chemistry. The quantitation of 2-deoxy-D-ribose under sodium ascorbate/H_2O_2 activation conditions is displayed in Figure 7, where it can be seen that the calculated production of hydroxyl radicals increases to about 700 nM at 60 min.

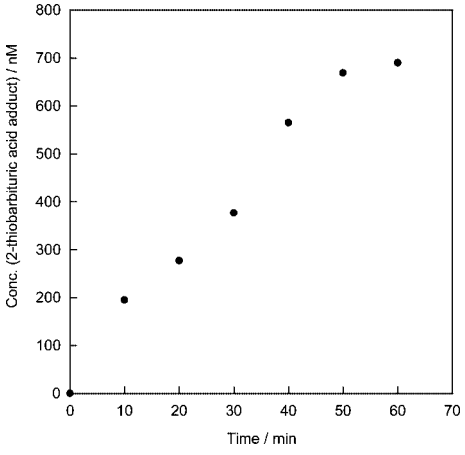

Figure 7. Production of hydroxyl radicals by $[Cu(ptO_2)(benz)]\cdot H_2O$ (**5**) as assayed by the 2-deoxy-D-ribose/2-thiobarbituric acid system.

In general, two mechanisms can be proposed for Cu^{II} complexes that mediate oxidative DNA cleavage, one involving hydroxyl radicals and another involving metal-oxido species. Bocarsly et al.[49,50,53] have suggested that hydroxyl radicals are generated by a variety of chemical and physical processes. Transition-metal-mediated hydroxyl radical production is known to occur by a number of routes; two well-known pathways are the Fenton and the Haber–Weiss mechanism. In the Fenton mechanism, the metal acts as a catalyst for hydroxyl radical generation from hydrogen peroxide:

$$Cu^{II}L + ascH_2 \rightarrow Cu^{I}L + ascH^-$$

$$Cu^{I}L + H_2O_2 \rightarrow Cu^{II}L + OH^- + OH^{\cdot}$$

whereas the Haber–Weiss reaction involves the reaction between superoxide anion and hydrogen peroxide:

$$Cu^{I}L + O_2 \rightarrow Cu^{II}L + O_2^-$$

$$O_2^- + H_2O_2 \rightarrow O_2 + OH^- + OH^{\cdot}$$

On the other hand, Sigman has suggested that bis(*o*-phenanthroline)copper(II), the classic nuclease system, follows a different mechanistic pathway.[54] Thus, reduction of the copper to cuprous state leads to the generation of superoxide anion. The O_2^- then dismutates to H_2O_2 and dioxygen and the hydrogen peroxide reacts with another equivalent of copper(I) to produce hydroxyl radical-like species, which may be bound to the metal. This species, which could be considered analogous to a metal-oxido species, is responsible for initiating DNA strand scission.[55]

Bocarsly et al. have compared their proposed mechanism with that of Cu-phenanthroline. They concluded that the differences between the two mechanisms are most likely related to the electronic differences between the ligands. Their mechanism is related to complexes with ligands that present σ character, while the mechanism proposed by Sigman is related to complexes with ligands that present π character (phen). Since the ptO_2^- and the ptN_2^- ligands in the title complexes present both σ and π character, both mechanisms can be proposed. This could explain why both hydroxyl radical scavengers and scavengers of singlet oxygen or singlet-oxygen-like species inhibit the DNA damage and strand breakage.

Conclusions

Ternary copper(II) complexes with 2,4,6-tri(2-pyridyl)-1,3,5-triazine hydrolytic derivatives have been prepared and structurally characterized with the aid of X-ray crystallography. The binding of DNA has been studied with the aid of viscosity and T_m measurements, which indicate that the complexes do not intercalate between the DNA base pairs. In contrast, an electrostatic interaction of the complexes with the phosphate backbone of the DNA can be deduced since the compounds are present in solution as the cationic $[Cu(ptO_2)]^+$ or $[Cu(ptN_2)]^+$ species. The complexes act as efficient chemical nucleases upon ascorbate activation. The participation of H_2O_2, hydroxyl radical, superoxide anion, and singlet-oxygen-like entities in the scission process mediated by the compounds suggests a mechanism pathway involving a Fenton or a Haber–Weiss reaction and copper(II)-oxene species.

Experimental Section

Materials and Physical Measurements: Reagents and solvents were commercially available and used without further purification. pUC18 was purchased from Roche Diagnostics. Calf-thymus DNA (CT-DNA) was supplied by Sigma–Aldrich.

Elemental analyses (C,N,H) were performed with a Carlo–Erba AAS instrument. IR spectra (KBr disks) were recorded with a Mattson satellite FT-IR spectrometer in the range 4000–400 cm^{-1}. Diffuse reflectance spectra (nujol mulls) of the complexes were recorded with a Shimadzu UV-2101 PC spectrophotometer. UV/Vis

spectra of the complex solutions were recorded with an HP 8453 spectrophotometer. FAB mass spectra were obtained with a VG Autospec spectrometer with 3-nitrobenzyl alcohol as matrix. EPR spectra were recorded at the X- and Q-band frequencies at room temperature with a Bruker ELEXSYS spectrometer. Electrochemical measurements were performed with the aid of a Princeton Applied Research Model 273A potentiostat/galvanostat. Cyclic voltammograms were obtained for acetonitrile solutions of the complexes with [TBA][ClO_4] as the supporting electrolyte under argon. The electrochemical cell employed had a standard three-electrode configuration, with a platinum working electrode, a platinum wire counter electrode, and an Ag/AgCl reference electrode.

[Cu(ptN$_2$)(OAc)]·3H$_2$O (1): An aqueous solution of $Cu_2Ac_4{\cdot}2H_2O$ (10 mL; 200 mg, 1 mmol) was added with continuous stirring to 40 mL of a yellow dmf solution of ptz (312 mg, 1 mmol). A dark green solution was formed immediately; after 30 min it turned blue-green in color and overnight it became blue with a small amount of violet precipitate. The precipitate was isolated by filtration, washed, and dried until constant weight. Yield: 20%. $C_{14}H_{19}CuN_5O_5$: calcd. C 41.94, H 4.77, N 17.47; found C 41.15, H 4.59, N 17.76.

Slow evaporation of the filtrate yielded blue, needle-like crystals that correspond to [Cu(ptO$_2$)(OAc)(H$_2$O)]·H$_2$O (**2**), which has previously been reported as [Cu(bpca)(OAc)(H$_2$O)]·H$_2$O.[26]

[Cu(ptN$_2$)(for)]·3H$_2$O (3) and [Cu(ptO$_2$)(for)(H$_2$O)] (4): An aqueous solution of [Cu$_2$(for)$_4$]·4H$_2$O (10 mL; 225 mg, 1 mmol) was added to 40 mL of a yellow dmf solution of ptz (312 mg, 1 mmol). A dark green solution was formed immediately; after 30 min it turned blue-green in color and overnight it became blue with a small amount of violet precipitate. The precipitate was isolated by filtration, washed, and dried until constant weight. Yield: 16%. $C_{13}H_{16}CuN_5O_5$: calcd. C 42.43, H 3.92, N 18.20; found C 42.43, H 4.14, N 18.12.

Slow evaporation of the filtrate yielded blue, needle-like crystals that correspond to [Cu(ptO$_2$)(for)(H$_2$O)] (**4**). Yield: 47%. $C_{13}H_{11}CuN_3O_5$: calcd. C 44.26, H 3.14, N 11.47; found calcd. C 44.10, H 3.09, N 11.90.

[Cu(ptO$_2$)(benz)]·H$_2$O (5): This compound was obtained by a procedure similar to that described above, but with $Cu_2(benz)_4$ (611 mg, 1, mmol), which was obtained either by mixing copper(II) perchlorate with sodium benzoate or by electrochemical synthesis. Slow evaporation of the resulting blue solution gave rise to blue, needle-like crystals after four or five days. Yield: 65%. $C_{19}H_{15}CuN_3O_5$: calcd. C 53.21, H 3.52, N 9.75; found C 52.99, H 3.44, N 9.75.

[Cu(ptO$_2$)F(H$_2$O)]·1.5H$_2$O (6): The synthesis of this compound is similar to that described above, but with $CuF_2{\cdot}2H_2O$ (137 mg, 1 mmol). Blue crystals formed 4 or 5 days after its preparation. Yield: 22%. $C_{12}H_{13}CuFN_3O_{4.5}$: calcd. C 40.74, H 3.70, N 11.88; found C 41.50, H 3.38, N 12.03.

X-ray Crystallography

[Cu(ptO$_2$)(for)(H$_2$O)] (4): Greenish-blue crystal, size $0.2\times0.2\times0.2$ mm, orthorhombic, space group $A2_1am$ (determined from the systematic absences). Data collection was performed at 293 K with a Nonius Kappa-CCD single crystal diffractometer, with Mo-K_α radiation (λ = 0.7173 Å). The crystal–detector distance was fixed at 45 mm, and a total of 148 images were collected by means of the oscillation method, with a scan angle per frame of 2° oscillation and a 10-s exposure time per image. Unit cell dimensions were determined from 895 reflections between θ = 2.91° and 27.49°. Unit cell parameters: a = 6.575(5), b = 13.462(5), c = 15.516(5) Å, V = 1373.4(12) Å^3, Z = 4, D_x = 1.701 mg m^{-3}, μ = 1.619 mm^{-1}. Multiple observations were averaged, R_{merge} = 0.000, resulting in 1533 unique reflections of which 1390 were observed with $I > 2\sigma(I)$. Final mosaicity was 0.42. Data completeness was 99.4%. All non-hydrogen atoms were refined anisotropically. Hydrogen atoms were located in the difference Fourier map and located geometrically. The final cycle of full-matrix least-squares refinement based on 1533 reflections and 131 parameters converged to a final value of $R1$ [$F^2 > 2\sigma(F^2)$] = 0.0291, $wR2$ [$F^2 > 2\sigma(F^2)$] = 0.0732, $R1$ (F^2) = 0.0338, $wR2$ (F^2) = 0.0754. The final difference Fourier maps showed no peaks higher than 0.323 e Å^{-3} at 1.56 Å from C32 and no troughs deeper than –0.513 e Å^{-3} at 0.72 Å from Cu1.

[Cu(ptO$_2$)(benz)]·H$_2$O (5): Violet crystal, size $0.8\times0.16\times0.008$ mm, monoclinic, space group $P2_1/a$ (determined from the systematic absences). Data collection was performed at 293 K with a Nonius Kappa-CCD single crystal diffractometer, with Mo-K_α radiation (λ = 0.7173 Å). The crystal–detector distance was fixed at 30.4 mm, and a total of 175 images were collected by means of the oscillation method, with a scan angle per frame of 1.7° oscillation and a 25-s exposure time per image. Unit cell dimensions were determined from 6088 reflections between θ = 0.998° and 33.142°. Unit cell parameters: a = 10.359(5), b = 10.295(5), c = 16.555(5) Å, β = 99.482(5)°, V = 1741.4(13) Å^3, Z = 4, D_x = 1.636 mg m^{-3}, μ = 1.293 mm^{-1}. Multiple observations were averaged, R_{merge} = 0.027, resulting in 6517 unique reflections of which 4279 were observed with $I > 2\sigma(I)$. Final mosaicity was 0.6. Data completeness was 98.5%. All non-hydrogen atoms were refined anisotropically. Hydrogen atoms were located in the difference Fourier map and located geometrically. The final cycle of full-matrix least-squares refinement based on 6517 reflections and 315 parameters converged to a final value of $R1$ [$F^2 > 2\sigma(F^2)$] = 0.0381, $wR2$ [$F^2 > 2\sigma(F^2)$] = 0.0887, $R1$ (F^2) = 0.0701, $wR2$ (F^2) = 0.0997. The final difference Fourier maps showed no peaks higher than 0.43 e Å^{-3} at 0.71 Å from C5 and no troughs deeper than 0.56 e Å^{-3} at 0.66 Å from Cu1.

[Cu(ptO$_2$)F(H$_2$O)]$_2$·3H$_2$O (6): Blue crystal, size $0.4\times0.25\times0.15$ mm, triclinic, space group $P\bar{1}$. Data collection was performed at 293 K with a Nonius Kappa2000 single crystal diffractometer, with Cu-K_α radiation (λ = 1.54184 Å). The crystal–detector distance was fixed at 35 mm, and a total of 261 images were collected by means of the oscillation method, with a scan angle per frame of 2° oscillation and 2-s exposure time per image. Unit cell dimensions were determined from 1136 reflections between θ = 0.999° and 47.840°. Unit cell parameters: a = 6.7680(4), b = 10.2740(5), c = 20.8690(10) Å, α = 98.635(2)°, β = 90.641(2)°, γ = 107.633(2)°, V = 1364.78(12) Å^3, Z = 2, D_x = 1.722 mg m^{-3}, μ = 2.621 mm^{-1}. Multiple observations were averaged, R_{merge} = 0.000, resulting in 1477 unique reflections of which 745 were observed with $I > 2\sigma(I)$. Final mosaicity was 0.65. Data completeness was 59.4%. All non-hydrogen atoms were refined anisotropically. Hydrogen atoms were located in the difference Fourier map and located geometrically. The final cycle of full-matrix least-squares refinement based on 1477 reflections and 407 parameters converged to a final value of $R1$ [$F^2 > 2\sigma(F)^2$] = 0.048, $wR2$ [$F^2 > 2\sigma(F^2)$] = 0.122, $R1$ (F^2) = 0.108, $wR2$ (F^2) = 0.162. The final difference Fourier maps showed no peaks higher than 0.36 e Å^{-3} at 0.92 Å from H3B and no troughs deeper than –0.37 e Å^{-3} at 0.31 Å from H2A.

Data collection for all complexes was performed with the program Collect.[56] Data reduction and cell refinement were performed with the programs HKL Denzo and Scalepack.[57] The crystal structure was solved by direct methods with the program SIR-97.[58] Aniso-

Table 3. Crystal and structure refinement data for [Cu(ptO$_2$)(for)(H$_2$O)] (**4**), [Cu(ptO$_2$)(benz)]·H$_2$O (**5**) and [Cu(ptO$_2$)F(H$_2$O)]$_2$·3H$_2$O (**6**).

	[Cu(ptO$_2$)(for)(H$_2$O)] (**4**)	[Cu(ptO$_2$)(benz)]·H$_2$O (**5**)	[Cu(ptO$_2$)F(H$_2$O)]$_2$·3H$_2$O (**6**)
Empirical formula	$C_{13}H_{11}CuN_3O_5$	$C_{19}H_{15}CuN_3O_5$	$C_{24}H_{26}Cu_2F_2N_6O_9$
Formula weight	351.78	428.88	707.59
Temperature [K]	293(2)	293(2)	293(2)
Wavelength [Å]	0.71069	0.71069	1.54184
Crystal system, space group	cba, $A2_1am$	monoclinic, $P2_1/a$	triclinic, $P\bar{1}$
a [Å]	6.575(5)	10.359(5)	6.7680(4)
b [Å]	13.462(5)	10.295(5)	10.2740(5)
c [Å]	15.516(5)	16.555(5)	20.8690(10)
α [°]	90.000(5)	90.000(5)	98.635(2)
β [°]	90.000(5)	99.482(5)	90.641(2)
γ [°]	90.000(5)	90.000(5)	107.633(2)
Volume [Å^3]	1373.4(12)	1741.4(13)	1364.78(12)
Z, calculated density [Mg m^{-3}]	4, 1.701	4, 1.636	2, 1.722
Absorption coefficient [mm^{-1}]	1.619	1.293	2.621
F(000)	712	876	720
Limiting indices	$8 \le h \le 8$	$-15 \le h \le 15$	$-6 \le h \le 6$
	$-17 \le k \le 17$	$-15 \le k \le 14$	$-9 \le k \le 9$
	$-19 \le l \le 20$	$-25 \le l \le 25$	$0 \le l \le 16$
Reflections collected/unique	1568/1533 [R_{int} = 0.0000]	10399/6517 [R_{int} = 0.0272]	2561/1477 [R_{int} = 0.0000]
Data/restraints/parameters	1533/2/131	6517/0/315	1477/3/407
Final R indices [$I > 2\sigma(I)$]	$R1$ = 0.0291, $wR2$ = 0.0732	$R1$ = 0.0381, $wR2$ = 0.0887	$R1$ = 0.0476, $wR2$ = 0.1218
R indices (all data)	$R1$ = 0.0338, $wR2$ = 0.0754	$R1$ = 0.0701, $wR2$ = 0.0977	$R1$ = 0.1079, $wR2$ = 0.1615

tropic least-squares refinement was carried out with SHELXL-97.[59] Geometrical calculations were made with PARST.[60] The crystallographic plots were made with ORTEP.[61] A summary of the crystallographic data of the complexes is given in Table 3.

CCDC-615303, -615304, and -615305 (for **4**–**6**, respectively) contain the supplementary crystallographic data for this paper. These data can be obtained free of charge from The Cambridge Crystallographic Data Centre via www.ccdc.cam.ac.uk/data_request/cif.

Viscosity Measurements: Viscosity experiments were carried out with a Cannon 25 L97 viscometer immersed in a Julabo thermostatted water bath maintained at 25.0 ± 0.1 °C. Solutions of the complexes (1–10 μM) in cacodylate buffer (pH 6.0) were added to a calf-thymus DNA (50 μM base pairs) solution in cacodylate buffer. The flow times were measured with a digital stopwatch. The flow measurements were performed in triplicate. Data are presented as $(\eta/\eta_0)^{1/3}$ vs. the ratio of the concentration of complex and DNA, where η is the viscosity of DNA in the presence of the complex and η_0 is the viscosity of DNA alone. Viscosity values were calculated from the observed flow time of a DNA-containing solution corrected for the flow time of buffer alone (t_0), $\eta = t - t_0$.

Thermal Denaturation Experiments: DNA-melting experiments were carried out by monitoring the absorbance (260 nm) of CT-DNA (100 μM base-pairs) at different temperatures in the absence and presence of the complexes in a 4:1 DNA/complex ratio. Measurements were performed with an Agilent 8453 UV/Vis spectrophotometer equipped with a Peltier temperature-controlled sample cell and driver (Agilent 89090A). The solution containing the ternary complex and CT-DNA in 0.1 M cacodylate buffer (2 mM NaCl, pH 6.0) was stirred continuously and heated with a rate of temperature increase of 1 °C min^{-1}. The temperature interval studied ranged from 25 to 90 °C.

pUC18 DNA Cleavage: A typical reaction with the complexes was undertaken by mixing 7 μL of 0.1 M cacodylate buffer (pH 6.0), 1 μL of pUC18 (0.25 μg μL^{-1}), 6 μL of a solution of the tested complex at increasing concentrations between 20 and 100 μM, and 6 μL of ascorbate (100-fold molar excess relative to the concentration of the complex) in cacodylate buffer. The mixtures were allowed to stand for 1 h at 37 °C, then 3 μL of a quench buffer solution consisting of 0.25% bromophenol blue, 0.25% xylene cyanole, and 30% glycerol was added. The solution was then subjected to electrophoresis on a 0.8% agarose gel in 0.5× TBE buffer (0.045 M tris, 0.045 M boric acid, and 1 mM EDTA) containing 2 μL per 100 mL of a solution of ethidium bromide (10 mg mL^{-1}) at 80 V for about 2 h. The gel was photographed on a capturing gel printer plus TDI.

To test for the presence of reactive oxygen species (ROS) generated during strand scission, various scavengers were added to the reaction mixtures. The scavengers used were Tiron (10 mM), DMSO (1 M), *tert*-butyl alcohol (1 M), potassium iodide (0.4 M), urea (0.4 M), sodium azide (100 mM), DABCO (0.4 M), and catalase (6.5 units). An assay in the presence of the minor groove binder distamycin (8 μM) and the major groove binder methyl green (2.5 μL of a 0.01 mg mL^{-1} solution) was also performed. Neocuproine, a ligand that chelates strongly to copper(I), was tested at 75 μM. Samples were treated as described above.

Hydroxyl Radical Assay by 2-Deoxy-D-ribose Degradation: Hydroxyl radical production by the complexes was assayed by degradation of 2-deoxy-D-ribose followed by quantitation of the 2-thiobarbituric acid adduct.[62] A 100 μM solution of metal complex was treated at room temperature with 4 mM 2-deoxy-D-ribose with activation by 50 mM sodium ascorbate and H_2O_2. Reactions were performed in a 4 mL volume of 0.1 M cacodylate buffer (pH 6.0). Reaction solutions were quenched with EDTA (2.4 mM final concentration) and stored in ice for 5 min. Each aliquot was then treated with 2-thiobarbituric acid (1.1 mM final concentration) at 95 °C for 15 min. The chromophore concentration was measured from its fluorescence intensity at 553 nm (excitation at 532 nm). The fluorescence intensity was used due to its sensitivity and also to the fact that ascorbate by-products absorb in the visible region and therefore interfere with visible quantitation of the thiobarbituric adduct. Fluorescence intensity was converted to concentration with a standard fluorescence curve constructed from known concentrations of the chromophore, synthesized from malondialdehyde and 2-thiobarbituric acid.[63] Blank reactions lacking a cleavage agent were included in each run and the blank intensity was subtracted from each experimental point.

Supporting Information (see also the footnote on the first page of this article): IR spectra of $[Cu(ptN_2)(for)]\cdot 3H_2O$ (**3**) and the $[Cu(ptO_2)(for)(H_2O)]$ (**4**; Figure S1); UV/Vis spectra of aqueous solutions of $[Cu(ptN_2)(OAc)]\cdot 3H_2O$ (**1**) and $[Cu(ptO_2)(OAc)(H_2O)]\cdot H_2O$ (**2**; Figure S2); EPR spectra of $[Cu(ptN_2)(for)]\cdot 3H_2O$ (**3**) and $[Cu(ptO_2)(for)(H_2O)]$ (**4**; Figure S3).

Acknowledgments

J. B., G. A., and J. L. G.-G acknowledge financial support from the Spanish Centro de Investigación Científica y Tecnólogica (CICYT) (CTQ2004-03735). M. G.-A. wishes to thank the city government of Valencia (Spain) for a Carmen and Severo Ochoa postdoctoral fellowship. B. M. acknowledges financial support from the Junta de Castilla y León (SA056A05).

[1] S. S. Wallace, *Int. J. Radiat. Biol.* **1994**, *66*, 579–589.
[2] K. Z. Guyton, T. W. Kensler, *Br. Med. Bull.* **1993**, *49*, 523–544.
[3] O. I. Arouma, B. Haliwell, E. Gajewski, M. Dizdaroglu, *Biochem. J.* **1991**, *273*, 601–604.
[4] M. Dizdaroglu, G. Rao, D. A. Beary, R. A. LaBiche, K. J. Hardy, *Arch. Biochem. Biophys.* **1991**, *285*, 317–324.
[5] S. E. Bryant, D. A. Vizard, D. A. Beary, R. A. LaBiche, K. J. Hardy, *Nucleic Acid Res.* **1981**, *9*, 5811–5823.
[6] C. D. Lewis, U. K. Laemli, *Cell* **1982**, *29*, 171–181.
[7] A. M. George, S. A. Sabovijev, L. E. Hart, W. A. Cramp, G. Harris, S. Homsey, *Br. J. Cancer* **1987**, *55*, 141–144.
[8] R. Stoewe, W. A. Prutz, *Free Rad. Biol. Med.* **1987**, *3*, 97–105.
[9] M. Dizdaroglu, O. I. Arouma, B. Haliwell, *Biochemistry* **1990**, *29*, 8447–8451.
[10] M. Masarwa, H. Cohen, D. Meyerstein, D. L. Hickman, A. Bakac, J. H. Espenson, *J. Am. Chem. Soc.* **1988**, *110*, 4293–4297.
[11] J. Sagripanti, K. H. Kraemer, *J. Biol. Chem.* **1989**, *264*, 1729–1734.
[12] K. Yamamoto, S. Kawanishi, *J. Biol. Chem.* **1989**, *264*, 15435–15440.
[13] G. R. A. Johnson, N. B. Nazat, R. A. Saadalla-Nazhat, *J. Chem. Soc., Faraday Trans. 1* **1988**, *84*, 501–510.
[14] N. C. Thomas, B. L. Iolcy, A. L. Rheingold, *Inorg. Chem.* **1988**, *27*, 3426–3429.
[15] S. Chirayil, V. Hegde, Y. Jahng, R. P. Thummel, *Inorg. Chem.* **1991**, *30*, 2821–2823.
[16] N. Gupta, N. Grover, G. A. Neyhart, P. Singh, H. B. Thorp, *Inorg. Chem.* **1993**, *32*, 310–316.
[17] R. M. Berger, J. R. Holcombe, *Inorg. Chim. Acta* **1995**, *232*, 217–221.
[18] R. M. Berger, D. D. Ellis II, *Inorg. Chim. Acta* **1996**, *241*, 1–4.
[19] E. M. Smolin, L. Rapoport, *S-Triazines and Derivatives*, Interscience, New York, **1959**, p. 163.
[20] E. I. Lerner, S. J. Lippard, *J. Am. Chem. Soc.* **1976**, *98*, 5397–5398.
[21] E. I. Lerner, S. J. Lippard, *Inorg. Chem.* **1977**, *16*, 1546–1551.
[22] J. Faus, M. Julve, J. M. Amigo, T. Debaerdemaeker, *J. Chem. Soc., Dalton Trans.* **1989**, 1681–1687.
[23] P. A. Gillard, P. A. Williams, *Transition Met. Chem.* **1979**, *4*, 18–23.
[24] P. Paul, B. Tyagi, M. M. Bhadbhade, E. Suresh, *J. Chem. Soc., Dalton Trans.* **1997**, 2273–2277.
[25] P. Paul, B. Tyagi, A. K. Bilakhiya, M. M. Bhadbade, G. Ramachandaiah, *Inorg. Chem.* **1998**, *37*, 5733–5742.
[26] X.-P. Zhou, D. Li, S.-L. Zheng, X. Zhang, T. Wu, *Inorg. Chem.* **2006**, *45*, 7119–7125.
[27] J. V. Folgado, E. Coronado, D. Beltrán-Porter, R. Burriel, A. Fuertes, C. Miratvilles, *J. Chem. Soc., Dalton Trans.* **1988**, 3041–3045.
[28] A. Cantarero, J. M. Amigo, J. Faus, M. Julve, T. Debaerdemaeker, *J. Chem. Soc., Dalton Trans.* **1988**, 2033–2039.
[29] J. V. Folgado, E. Martinez-Tamayo, A. Beltrán-Porter, D. Beltrán-Porter, *Polyhedron* **1989**, *8*, 1077–1083.
[30] A. Kamiyama, T. Noguchi, T. Kajiwara, T. Ito, *Inorg. Chem.* **2002**, *41*, 507–512.
[31] T. Glaser, T. Lugger, R. Fröhlich, *Eur. J. Inorg. Chem.* **2004**, 394–400.
[32] B. Casellas, F. Constantino, A. Mandonnet, A. Caneschi, D. Gatteschi, *Inorg. Chim. Acta* **2005**, *358*, 177–185.
[33] S. A. Cotton, V. Franckevicius, M. F. Mahon, L. L. Ooi, P. R. Raithby, S. A. Teat, *Polyhedron* **2006**, *25*, 1057–1068.
[34] S. R. Dey, C. R. Choudhury, S. P. Dey, D. K. Dey, N. Mondal, S. O. G. Mahalli, K. M. A. Malik, S. Mitra, *J. Chem. Res. (S)* **2002**, 496–499.
[35] T. Kawijara, A. Kamiyama, T. Ito, *Chem. Commun.* **2002**, 1256–1257.
[36] N. Gupta, N. Grover, G. A. Neyhart, P. Singh, H. B. Thorp, *Inorg. Chem.* **1993**, *32*, 310–316.
[37] M. González-Álvarez, G. Alzuet, J. Borrás, B. Macías, M. Del Olmo, M. Liu-González, F. Sanz, *J. Inorg. Biochem.* **2002**, *89*, 29–35.
[38] B. Macías, I. García, M. J. Villa, M. González-Álvarez, J. Borrás, A. Castiñeiras, *J. Inorg. Biochem.* **2003**, *96*, 367–374.
[39] M. González-Álvarez, G. Alzuet, J. Borrás, B. Macías, A. Castiñeiras, *Inorg. Chem.* **2003**, *42*, 2992–2998.
[40] M. González-Álvarez, G. Alzuet, J. Borrás, M. Pitié, B. Meunier, *J. Biol. Inorg. Chem.* **2003**, *8*, 644–652.
[41] B. Macías, M. V. Villa, F. Sanz, J. Borrás, M. González-Álvarez, G. Alzuet, *J. Inorg. Biochem.* **2005**, *99*, 1441–1448.
[42] R. Cejudo, G. Alzuet, M. González-Álvarez, J. L. García-Giménez, J. Borrás, M. Liu-González, *J. Inorg. Biochem.* **2006**, *100*, 70–79.
[43] A. W. Addison, T. N. Rao, J. Reedijk, J. van Rijn, C. G. Verschoor, *J. Chem. Soc., Dalton Trans.* **1984**, 1349–1356.
[44] G. A. Jefrey, *An Introduction to Hydrogen Bonding*, Oxford University Press, Oxford, **1997**.
[45] WINEPR-Simphonia 1. 25 Bruker Analytic Gmbh, Kalrsruhe, Germany, **1994–96**.
[46] J. Liu, T. Zhang, L. Que, H. Zhou, Q. Zhang, J. Liangnian, *J. Inorg. Biochem.* **2002**, *91*, 269–276.
[47] A. Mazumder, C. L. Sutton, D. S. Sigman, *Inorg. Chem.* **1993**, *32*, 3516–3560.
[48] S. H. Chiou, N. Ohtsu, K. G. Bensch, in *Biological and Inorganic Copper Chemistry* (Eds.: D. Karlin, J. Zubieta), Adenine Press, New York, **1985**, pp. 119–123.
[49] C. A. Detmer III, F. V. Pamatong, J. R. Bocarsly, *Inorg. Chem.* **1996**, *35*, 6292–6298.
[50] C. A. Detmer III, F. V. Pamatong, J. R. Bocarsly, *Inorg. Chem.* **1997**, *36*, 3676–3682.
[51] C. J. Burrows, J. G. Muller, *Chem. Rev.* **1998**, *98*, 1109–1152.
[52] B. Haliwell, J. M. C. Gutteridge, in *CRC Handbook of Methods for Oxygen Radical Research* (Ed.: R. A. Greenwald), CRC Press, Boca Raton, FL, **1985**, p. 177.
[53] F. V. Pamatong, C. A. Detmer III, J. R. Bocarsly, *J. Am. Chem. Soc.* **1996**, *118*, 5339–5345.
[54] D. R. Graham, L. E. Marshall, K. A. Reich, D. S. Sigman, *J. Am. Chem. Soc.* **1980**, *102*, 5419–5421.
[55] D. S. Sigman, *Acc. Chem. Res.* **1986**, *19*, 180–186.
[56] COLLECT, Nonius BV, **1997–2000**.
[57] DENZO-SCALEPACK, Z. Otwinowski, W. Minor, *"Processing of X-ray Diffraction Data Collected in Oscillation Mode"*, Methods in Enzymology, Volume 276: Macromolecular Crystallography, part A, p. 307–326 (Eds.: C. W. Carter Jr, R. M. Sweet), Academic Press, **1997**.
[58] SIR97: A. Altomare, M. C. Burla, M. Camalli, G. L. Cascarano, C. Giacovazzo, A. Guagliardi, A. G. G. Moliterni, G. Polidori, R. Spagna, *J. Appl. Crystallogr.* **1999**, *32*, 115–119.

[59] SHELX97, G. M. Sheldrick, *SHELX97. Programs for Crystal Structure Analysis (Release 97-2)*, University of Göttingen, Germany, **1997**.
[60] PARST: a) M. Nardelli, *Comput. Chem.* **1983**, *7*, 95–97; b) M. Nardelli, *J. Appl. Crystallogr.* **1995**, *28*, 659.
[61] ORTEP3 for Windows: L. J. Farrugia, *J. Appl. Crystallogr.* **1997**, *30*, 565.
[62] B. Halliwell, J. M. C. Gutteridge, in CRC *Handbook of methods for Oxygen Radical Research* (Ed.: R. A. Greenwald), CRC Press, Boca Raton, FL, USA, **1985**, p. 177.
[63] R. M. Burger, A. R. Berkowith, J. Peisach, S. B. Horwitz, *J. Biol. Chem.* **1980**, *255*, 11832–11838.

Received: September 5, 2006
Published Online: January 12, 2007

